This article has been accepted for publication in a future issue of this journal, but has not been fully edited. Content may change prior to final publication. Citation information: DOI 10.1109/TWC.2020.3016962, IEEE Transactions on Wireless Communications

Real-time Prediction of Non-stationary Wireless Channel

Maqsood Abdul Careem and Aveek Dutta
Department of Electrical and Computer Engineering
University at Albany SUNY, Albany, NY 12222 USA
{mabdulcareem, adutta}@albany.edu

***Abstract*—Modern wireless systems are increasingly dense and dynamic that makes the channel highly non-stationary, rendering conventional receivers sub-optimal in practice. Predicting the channel characteristics for non-stationary channels has the distinct advantage of pre-conditioning the waveform at the transmitter to *match* the expected fading profile. The difficulty lies in extracting an accurate model for the channel, especially if the underlying variables are uncorrelated, unobserved and immeasurable. Our work implements this prescience by assimilating the Channel State Information (CSI), obtained as feedback from the receiver, over time and space to adjust the modulation vectors such that the channel impairments are significantly diminished at the receiver, improving the Bit Error Rate (BER). We design a channel recommender, in which an adaptive smoother is used to filter the noise in CSI, while a tensor factorization & completion approach is used to track the ephemeral changes in non-stationary channel statistics by observing the changes in certain measurable parameters. V2X communication is used as an example of non-stationary channels to shows the efficacy of this approach. Overall, the system is shown to operate with a prediction accuracy of 10^{-3} MSE even in dense scattering environments over space and time, improving the BER at the receiver by 90% for higher-order modulations.**

I. Introduction

Design of optimal receivers using conventional communication theory, rely on mathematical and statistical channel models that describe how a signal is corrupted during transmission. In particular, communication techniques such as modulation, coding, and detection that mitigate performance degradation due to channel impairments are based on such channel models and, in some cases, instantaneous channel state information. However, there are many propagation environments where this approach does not work well because the underlying physical channel is highly dimensional, poorly understood, nonlinear or non-stationary. These channels lead to sub-optimal and sometimes catastrophic performance using conventional receivers [1]. This problem is relatively tractable and has been studied in the literature for linear, stationary channels with normal distribution by employing a gamut of mathematical tools for Bayesian inference such as Autoregressive random walks, Kalman filters and Particle filters.

While it is desirable to learn the behavior of the wireless channel, it is a non-trivial problem in practice. Wireless channels are influenced by many external variables that are often correlated, time-dependant or unknown. Thus, any acquired knowledge about these factors will inevitably be ephemeral, which necessitates long-term learning models that are fast, adaptive and evolve over time. Further, in multicarrier communication systems like OFDM, frequency selective fading can be alleviated if the subcarriers are pre-equalized in accordance to the impending channel response [2], [3]. Therefore, we show that in non-stationary channels, the transmitter has to *learn and predict* the most accurate channel response on a per-packet (or even per-symbol) basis such that when the signal is pre-equalized by the *inverse* of the channel it counteracts the effects of the wireless channel.

Recommender systems are designed to bridge the gap between the desired and actual behavior of a partially known (or sometimes unknown) process by iteratively tracking certain patterns in the outcomes. In turn, this reduces the ambiguity and uncertainty in the decision making process for the end-user. Wireless communication over non-stationary channel, is analogous to such a recommender system, where the receiver can significantly reduce its packet (or bit) error rate, only if the transmitter uses the *recommended* signal parameters based on historically observed channel profiles, obtained as a feedback from the receivers. Intuitively, if the transmitter pre-conditions the waveform with the mathematical *inverse* of the expected channel, the received signal will likely contain minimal amount of distortion.

We use V2X (Vehicle (V) to Everything (X)) channels as an example of highly non-stationary channels to validate the efficacy of predictive analytics at the transmitter. Recent explosion in autonomous vehicles [4] has renewed the interest in investigating the properties of the vehicular wireless channel for low-latency, broadband communication [5]. Vehicular networks are unique because the communicating nodes are always moving relative to each other. Consequently, the wireless channel is extremely volatile, which is a combination of many factors like, Doppler shift, shadowing, scattering (large and small scale), etc. More importantly, all of these quantities are time-varying and statistically non-stationary [6], [7]. A reliable wireless channel also provides resiliency in higher-layer network functions like traffic-aware, low-latency caching of content and coordinated downlink transmission for multiuser communication techniques like MU-MIMO.

Our goal in this work is to rely on a set of measurable parameters (denoted by $\mathfrak{M}$) like the vehicle density (N_s), vehicle location, mapped into quasi-stationary segments (S) [8] and the CSI feedback (CSI) to construct a non-uniformly spaced, non-stationary time series (indexed by time of reception, T). The CSI from the receivers captures a wide variety of channel characteristics across a stretch of road under different scattering environments. Broadband communication using frequency domain modulation such as OFDM used in the standards advocated for WAVE [9] also captures the channel profile in frequency domain. Although, V2X is an extreme

This article has been accepted for publication in a future issue of this journal, but has not been fully edited. Content may change prior to final publication. Citation information: DOI 10.1109/TWC.2020.3016962, IEEE Transactions on Wireless Communications

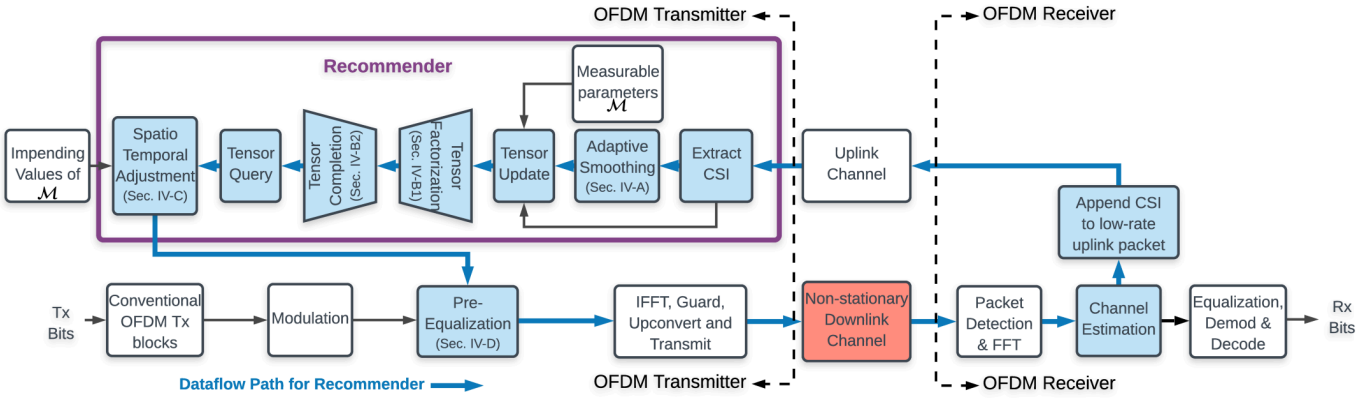

Figure 1: System view of the Channel Recommender framework at the transmitter for predicting non-stationary channel. The transmitter and receiver work together to lower the BER. Corresponding sections for description are indicated within text.

example of non-stationary channel, the method discussed is organically applicable to other non-stationary wireless channels with similar properties, like 802.11-(xx), High-speed train (HST) communication, Massive MIMO and mmWave networks with small-scale fading characteristics [10], [1], [11], by considering the available set of measurable parameters (further discussed in Section VI). Figure 1 shows the channel recommender system for V2X communication. It operates on the quadruplet, $[CSI, N_s, S, T]^i$, obtained from vehicle i.

System Description: The Recommender framework involving the transmitter, non-stationary channel and the receiver is shown in figure 1. *The flow of information from transmitter to the receiver is as follows:* At the transmitter, the bits that are to be transmitted are modulated (using standard OFDM modulation schemes) to generate the I/Q vectors. These I/Q vectors are pre-equalized with the most accurate prediction of the impending channel profile produced by the Recommender. The pre-equalized I/Q vectors are converted to time-domain waveform and transmitted over the non-stationary downlink channel. At the receiver, the baseband signal is estimated using conventional pilot based estimation, equalized, demodulated and decoded to extract the information bits.

In parallel, *the Recommender at the transmitter works as follows:* The CSI is piggy-backed on a low-rate uplink packet (e.g., acknowledgement packet) and is extracted at the transmitter and transformed to the measurement channel. The first step is to pre-process the CSI using an adaptive filter (e.g., a combination of autoregression (AR) and Kalman filter [12], [13]), to track the long-term channel statistics and dampen the effects of non-linearities in the estimation process in the receiver and the uplink channel (as explained in Section IV-A). The tracked channel statistics is used in the second step to predict the accurate downlink channel profile for any target receiver, according to its position and the scattering environment. This is accomplished by constructing a channel tensor (referred to as the *tensor update* stage) to store the CSI (represents the corresponding error in the predicted channel) and the transitions in other measurable parameters, denoted by the set $\mathcal{M}$ (e.g., $\mathcal{M}$=$\{N_s, S\}$, with number of scatterers, N_s and location of receiver, S), from the last observed CSI in time-step k. The tensor, $\mathcal{Z}$ is sparse, as all entries may not have been observed as well as noisy due to correlated latent variables. Thus, the tensor is factorized into its latent representation and reconstructed to generate the output tensor $\hat{\mathcal{Z}}$ (as described in Section IV-B), which is complete and less noisy and represents future states of the channel for impending values of the measurable parameter set $\mathcal{M}$. In the *tensor query* stage, the recommended downlink profile is extracted from $\hat{\mathcal{Z}}$ corresponding to the impending values of $\mathcal{M}$. The outputs of the adaptive smoother and tensor factorization & completion are fused to track and accurately predict the long term and short-term transients in the channel profile (as explained in Section IV-C). After this adjustment, the final step is to pre-condition the waveform, such that the receiver estimates an almost flat fading across all subcarriers (in Section IV-D). This step eliminates the need for any complex receiver side algorithm [14] and is also compatible with conventional pilot based equalization. As the recommender system evolves with more spatio-temporal CSI, the gap between the predicted and the true channel gets asymptotically small leading to almost two orders of magnitude improvement in the BER for QAM modulations. The results in Section V show the various trade-offs and efficacy of the channel recommender for non-stationary channels, and compares its performance with state-of-the-art receiver-side equalization and transmitter-side channel prediction techniques.

II. Related Work

The propagation environment in modern wireless systems like V2X [15], HST [16], mobile Massive MIMO [17] and modern mmWave networks [10], [11] are shown to be inherently non-stationary, due to the distance-dependent path loss, shadowing, delay or Doppler drift and time-varying propagation scenarios [18]. Consequently, such non-stationary channels are particularly difficult to analyze [19], [20]. This nature impacts the reliability and latency of data transmission [15], which has been validated by various measurement campaigns [7]. Significant prior research exist on channel models for modern non-stationary wireless systems [11], [17], that typically build on geometric stochastic channel models by capturing the temporal evolution of small-scale fading channel characteristics. A unified framework of 3-D non-stationary channels is presented in [11], which is based on array-time

This article has been accepted for publication in a future issue of this journal, but has not been fully edited. Content may change prior to final publication. Citation information: DOI 10.1109/TWC.2020.3016962, IEEE Transactions on Wireless Communications

cluster evolution of the channel statistics of the WINNER II channel model. The degree of non-stationarity of wireless channels is evaluated using metrics to assess the rate of variation of certain local channel statistics such as variation of the power delay profile [21], or using a correlation matrix distance measure [22]. [22] showed that significant changes in the spatial structure of the mobile radio channels appear even for small movements within an indoor environment, making indoor MIMO radio channels non-stationary. However, reliable communication over non-stationary channels is very rare in literature, due to the challenging nature of tracking such channel statistics.

A collection of classical techniques for estimation, equalization and algebraic coding for fast varying channels is presented in [23], mostly under the assumption of WSSUS (Wide-Sense Stationary Uncorrelated Scattering) channels. In practice, the WSSUS condition is never satisfied exactly, due to the existence of nonstationary channel fluctuations [18]. State-of-the-art communication receivers have relied on post equalization techniques such as Decision Feedback Equalizers (DFE) [24], [25] for time varying channels at the cost of added receiver complexity and complex feedback paths. Channel estimation of fast varying vehicular channels in [26] relied on extended Kalman filters, but is restricted to a deterministic evolution of the channel (multi-path Rayleigh model). Channel prediction in the literature leverage Parametric Radio Channel (PRC) models, Basis-Expansion Models (BEM) or Autoregressive (AR) models. PRC methods assume that the underlying multipath parameters causing fading vary much slower, and leverage channel extrapolation to determine the channel states [27]. BEM channel models use orthogonal basis to describe the channel [28]. AR models treat the channel as a linear combination of known channel coefficients and applies filtering techniques (e.g., minimum mean squared error (MMSE), and Kalman filtering [12], [13], [29]) with the knowledge of the channel correlation matrix to predict future CSI. While these methods are used to predict channels with known or unknown distributions, they are not capable of predicting the ephemeral variations in non-stationary channels and are detrimental for higher-order modulations (explained in Section IV-A). A comparison of the proposed channel recommender with state-of-the-art predictive and reactive techniques is presented in Section V.

In the context of wireless networks, recommender systems have been adopted in network traffic data [30], wireless channel selection [31] and IoT [32], but not for channel prediction. To the best of our knowledge channel prediction for general non-stationary wireless channel has not been studied in the literature. We design a unified framework for non-stationary channel prediction using a spatio-temporal recommender, in which an adaptive pre-smoother tracks the long term channel evolution, while the tensor factorization & completion tracks the ephemeral changes in channel statistics by observing the changes in measurable parameters. This research builds this prescience in a transmitter making ultra low latency applications reliable by pre-compensating the waveform according to the impending channel impairments. This emphasizes the challenging nature of the problem and the novelty of this work.

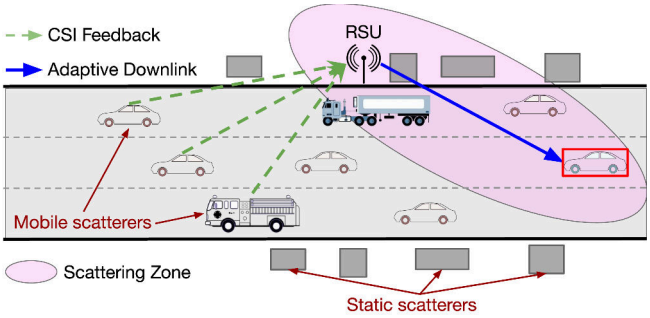

Figure 2: Example of V2X communication: Scattering zone (shown by ellipse) between the RSU (Road-side Unit) and vehicle consists of stationary and mobile scatterers, making the channel non-stationary over time and frequency.

III. Background and Known Results

Characteristics of non-stationary wireless channels: A wireless channel is typically modeled as a random process. When the statistics (mean and variance) of the channel distribution are functions of time, it is referred to as a non-stationary channel. In contrast to commonly known channel models, that are assumed to be stationary stochastic processes, non-stationary links contain much richer and complex set of variables [33], [34]. Examples like V2X channels are crippled by multiple paths resulting from reflection and scattering from various objects in the vicinity [15], like large scale scattering from roadside features and small scale scattering from other nearby vehicles. This is further affected by the mobility of the vehicles, which causes the scattering environment to change with the position of the vehicle. On the other hand, small scale scattering depends on topological factors, such as traffic density, shape (geometry) of the vehicles and speed. Also, weather related factors such as absorption and rain-attenuation is another factor that is unpredictable and destroys the integrity of the waveform. The combined effect of these factors is reflected on the wireless signal and contains all the information necessary to learn about these features over time.

Consider the vehicular environment shown in figure 2, where a transmitter (RSU or a vehicle) is communicating with a target vehicle (vehicle in red box in figure 2) equipped with a single isotropic antenna through a multipath environment. The road is divided into several *segments*, where each segment has its own unique propagation characteristics and represents a period of quasi-stationarity, during which the probability distributions of the large scale scatterers, like road-side features, do not change noticeably [8], [35].

The scattering zone represents a single-link connecting the transmitter and receiver, and is geometrically represented by an ellipse [8]. In each segment, there are two types of scatterers: *fixed scatterers*, which are usually along the side of the road, like buildings and sign posts, and *variable scatterers*, which are usually on the road, like vehicles. While the number of fixed scatterers per segment is a fixed scalar, the number of variable scatterers per segment is modeled as a random variable whose expected value is a measure of the vehicle density in the road segment. When the scattering environment changes, some of the large scale parameters (LSPs) and small scale

This article has been accepted for publication in a future issue of this journal, but has not been fully edited. Content may change prior to final publication. Citation information: DOI 10.1109/TWC.2020.3016962, IEEE Transactions on Wireless Communications

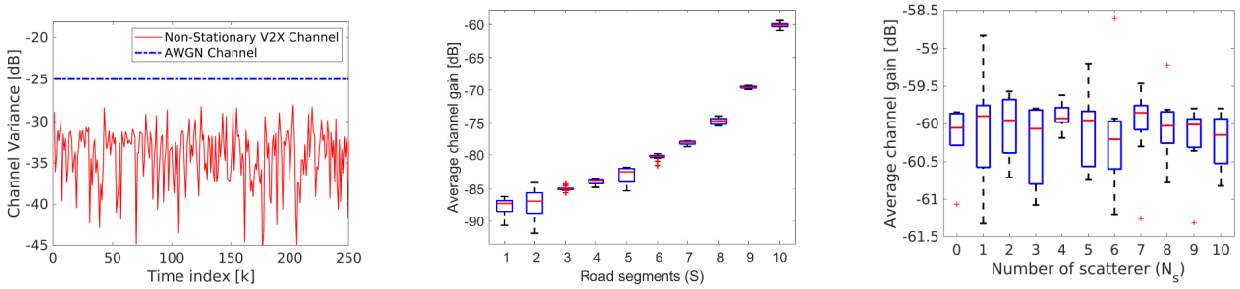

(a) Variance of channel gain with time (constant N_s and S)

(b) Spatial Distribution of channel gain (constant N_s)

(c) Variation of channel gain with scatterer density (constant S)

Figure 3: Non-stationarity of the V2X channel over time, space and vehicle density with a static transmitter at 10$^{\text{th}}$ segment: a) Variance of the channel gain is a function of time even with constant scattering and static receiver (N_s=5, S=5), while variance of AWGN channel is constant, b) Channel variance is a function of time for constant scatterers (N_s=5) across road segments, and c) Non-stationarity of the channel variance with number of scatterers for receivers within same road segment (S=5).

parameters (SSPs) also change accordingly, resulting in a new and unique channel profile (coefficients) and consequently, new power-delay and power-frequency profiles as well.

Non-stationary channels can be modeled as Geometry-based Stochastic Channel Models (GSCM) [8], which forms the basis of the widely used WINNER channel model. The non-stationary V2X channel at time k and for the n^{th} OFDM subcarrier is given by (1),

$$h(k,n) = \sum_{\ell=1}^{N_s(k)} h(k,n,\ell) \quad \text{where,} \tag{1}$$

$$h(k,n,\ell) = \sum_{m=1}^{M_\ell} \alpha_m e^{j\varphi_m} e^{j2\pi f_{D_m} k} \delta(\tau-\tau_m)\delta(\theta-\theta_m)\delta(\phi-\phi_m)$$

where, $N_s(k)$ is the number of scatterers assuming that at time k, each resolvable path corresponds to one scatterer, and M is the number of sub-paths constituting each ray. $\alpha_m(k,n)$ is the complex channel gain at time k and subcarrier n. $\phi_m(k,n)$ and $\theta_m(k,n)$ are the angle of departure (AoD) and the angle of arrival (AoA) of the m^{th} sub-path respectively. $f_{D_m}(k,n)$ is the Doppler frequency and $\tau_m(k,n)$ is the path delay measured at time k for subcarrier n, which depend on the scatterers' locations. The AoAs and AoDs are functions of the transmitter (e.g., RSU or vehicle) location, receiver (e.g., vehicle) location, and number of scatterers in each scattering zone that are stochastically distributed [13]. The path delay (and consequently the channel impulse response) collectively depend on these factors. Thus, *the channel dynamics are functions of the number of scatterers and their locations with respect to the transmitter and the receiver, and the mobility of the receiver*. This non-stationarity over space, time and vehicular density affects the reliability and latency of data transmission, which has been validated by various measurement campaigns [6].

Figure 3 shows the non-stationarity of the statistics (mean and variance) of the channel gain (averaged over all subcarriers) for an example V2X propagation environment using the simulation framework in Section V-A. Figure 3a shows that the variance of the channel gain is time varying, for a static vehicle with fixed scattering. Figures 3b and 3c show that the average channel gain (and variance) is a function of the location of the reporting vehicle and its scattering environment. The average channel gain in figure 3b is higher when the receiver is in the vicinity of the transmitter. The dependence of the mean and variance of the channel gain on time, location, frequency and scatterer density lends to the high non-stationarity of the channel. This non-stationary channel is reported as CSI feedback by the receiver, which serves as the input to the recommender in figure 1. In contrast for AWGN channel (an example of a stationary channel), the channel variance is constant over time and the channel statistics does not depend on the receiver location or scattering environment. The goal is to predict this non-stationary channel profile at the transmitter and pre-condition the waveform to offset the effect of such impairments.

Role of Channel State Information (CSI): CSI in OFDM based systems, can be interpreted as the time-average of the estimated frequency domain complex channel coefficients at the receiver over the duration of the packet (typically many OFDM symbols). Therefore, CSI information comprises of real and imaginary values for all subcarriers (typically represented by 12 to 16 bits in a fixed point implementation of a transceiver). This information is easily piggy-backed onto the acknowledgment frames (only adds 64 subcarriers×16 bits per subcarrier×2 I/Q=256 bytes of overhead[1]) which are usually modulated using low rate constellation like BPSK for robust uplink communication. Therefore, the CSI is essentially a feedback information from the receiver that captures the fading profile of the downlink channel. In general, the CSI can be used by the transmitter to tune the parameters (rate adaptation) of future packets. However, this is only feasible if the channel is changing at a slow rate. From figure 3, it is evident that non-stationary links are an exception to this. Simply because, by the time the CSI arrives at the transmitter, piggy-backed on the acknowledgment frame, the channel has already changed to a new state and the CSI is rendered ineffective for any adaptive transmission. This is a serious drawback for transmitter encoding like rateless code [36], as it depends on automatic repeats like HARQ to adjust the coding parameters. The rapid changes in non-stationary channel forces

[1] In general for MIMO-OFDM systems, the CSI is an m_{tx}×m_{rx}×W data structure, where m_{tx} and m_{rx} are the number of transmit and receive antennas, and W is the number of OFDM subcarriers used in the system.

This article has been accepted for publication in a future issue of this journal, but has not been fully edited. Content may change prior to final publication. Citation information: DOI 10.1109/TWC.2020.3016962, IEEE Transactions on Wireless Communications

the transmitter and receiver algorithms to act on *stale* channel states leading to severely degraded performance as shown in figure 4b. In contrast, predictive analytics using large number of CSI measurements, facilitates linear channel estimation and equalization at the receiver to produce a flat response across subcarriers, which ultimately improves the BER (Section V).

IV. Channel Recommendation System

The CSI is a quantized estimate of the downlink channel that can be used to adjust the I/Q modulation vectors for future transmissions. However, the high dynamics of the non-stationary channels requires agile scheduling of packets at the transmitter for links with different parameters (e.g, agile scheduling for different scattering environment and location for V2X links). Hence, the CSI may become obsolete (without further processing), and the transmitter has the added burden of making unique predictions for every downlink packet.

To address the problem of predicting the non-stationary wireless channel we design a channel recommender that has four stages as shown in figure 1: *A) Adaptive Smoothing:* The first step is to accumulate the CSI from the receivers and iteratively track the temporal evolution of the channel and smooth the noise in the CSI, *B) Tensor Factorization & Completion:* This step generates channel recommendations to account for the change in the measurable parameters (scattering environment and location of vehicles) over time [37]. This involves using the accumulated CSI along with other measurable parameters that might affect channel states, to analyze the correlation among the variables that constitute the measured CSI. This information is utilized to obtain an accurate representation of the channel based on the impending (future) states of the observable variables. *C) Spatio-Temporal Adjustment:* The output of steps A and B is fused to form the predicted downlink channel profile for the next packet, and *D) Pre-Equalization:* The downlink waveform is pre-equalized using the predicted channel profile, to achieve flat fading at the receiver. For example, in V2X communication the transmitter (RSU) processes the channel state, received as a quadruplet $[CSI, N_s, S, T]^i$ for each vehicle i, whenever it is available. It is to be noted that any two CSI (typically piggy-backed on an acknowledgement packet) are statistically different even if the other values in the quadruplet remain unchanged. The recommender system operates in real-time, requires minimal training and lowers the BER even when the tensor is 99% sparse and contains noisy measurements.

A. Adaptive Smoothing

The adaptive smoothing step mitigates the non-stationary noise in the channel and tracks the temporal evolution of the channel. The Kalman filter is particularly suited for tracking the channel statistics of non-stationary channels represented by (1), since it is a linear system. However, instead of tracking the channel coefficients (per subcarrier) using a Kalman filter, the tracked channel coefficients are combined by an autoregressive (AR) model and the weights of the AR model are tracked by the Kalman filter [12]. Table I shows the meaning and dimensions of the variables used in the adaptive smoother. A noisy AR process (random walk) of order p in (2) has the corresponding state-space representations (3) and (4).

Table I: Variables used in Adaptive Smoothing algorithm

Variable	Dimension	Meaning
$\mathbf{a}(k)$	$pN\times1$	AR-model coefficients vector
$\mathbf{u}_1(k)$	$pN\times1$	Gaussian process noise vector, $\mathcal{N}(0, \sigma^2_{u1})$
$\mathbf{u}_2(k)$	$N\times1$	Gaussian measurement noise vector, $\mathcal{N}(0, \sigma^2_{u2})$
$\mathbf{z}(k)$	$N\times1$	Measurement channel vector
$\mathbf{z}_p(k)$	$N\times1$	Predicted channel vector
$\mathbf{C}(k-1)$	$N\times pN$	Measurement matrix
$\mathbf{R}_{u_1}(k)$	$pN\times pN$	Process noise covariance matrix
$\mathbf{R}_{u_2}(k)$	$N\times N$	Measurement noise covariance matrix
$\mathbf{R}_p(k)$	$pN\times pN$	Predicted state-error covariance matrix
$\tilde{\mathbf{R}}_c(k+1)$	$pN\times pN$	Corrected state-error covariance matrix
$\mathbf{R}_c(k+1)$	$pN\times pN$	Upper-triangular portion of $\tilde{\mathbf{R}}_c(k+1)$
$\mathbf{G}(k)$	$pN\times N$	Kalman gain matrix
$\mathbf{I}$	$pN\times pN$	Identity matrix
$\mathbf{c}_k$	$pN\times1$	Smoothing Coefficients vector

$$z(k) = \sum_{i=1}^{p} a_i z(k-i) + u(k) \tag{2}$$

where, $\{a_i, 1 \le i \le p\}$ are the weights that represent the statistics of the time series, and $u(k)$ is an additive white noise.

$$\mathbf{a}(k+1) = \mathbf{a}(k) + \mathbf{u}_1(k) \tag{3}$$

$$\mathbf{z}(k) = \mathbf{C}(k-1)\mathbf{a}(k) + \mathbf{u}_2(k) \tag{4}$$

$\mathbf{a}(k)$ is the coefficients vector (statistics of the channel realizations) of the AR model to be tracked using Kalman filter at time k for N subcarriers, and $\mathbf{z}(k)$ is the measurement channel vector. $\mathbf{C}(k-1)$ maps the state space into the observation space as given by (5),

$$\mathbf{C}(k-1) = \text{diag}\{\mathbf{z}(k-1, n), 1 \le n \le N\} \tag{5}$$

where, $\mathbf{z}(k-1, n)=[z(k-1, n), z(k-2, n), \ldots, z(k-p, n)]$ is a vector containing the previous p CSI that were piggybacked on prior acknowledgment frames as shown in figure 1.

The formulation of the Kalman filter algorithm that is used to track the AR-parameters is as follows:

- Prediction step:

$$\mathbf{R}_{u_1}(k) = \mathbb{E}[\mathbf{u}_1(k)\mathbf{u}_1^H(k)] \tag{6}$$

$$\mathbf{R}_{u_2}(k) = \mathbb{E}[\mathbf{u}_2(k)\mathbf{u}_2^H(k)] \tag{7}$$

$$\mathbf{G}(k)=\mathbf{R}_c(k)\mathbf{C}^H(k-1)[\mathbf{C}(k-1)\mathbf{R}_c(k)\mathbf{C}^H(k-1)+\mathbf{R}_{u_2}(k)]^+ \tag{8}$$

$$\mathbf{R}_p(k) = \big(\mathbf{I} - \mathbf{G}(k)\mathbf{C}(k-1)\big)\mathbf{R}_c(k) \tag{9}$$

- Correction step:

$$\mathbf{a}(k+1) = \mathbf{a}(k) + \mathbf{G}(k)\big(\mathbf{z}(k) - \mathbf{C}(k-1)\mathbf{a}(k)\big) \tag{10}$$

$$\tilde{\mathbf{R}}_c(k+1) = \mathbf{R}_p(k) + \mathbf{R}_{u_1}(k) \tag{11}$$

$$\mathbf{R}_c(k+1) = \text{Triu}(\tilde{\mathbf{R}}_c(k+1)) \tag{12}$$

where, X^+ is the pseudo-inverse of matrix X, and $\text{Triu}(X)$ is the upper-triangular portion of X. The upper-triangular portion of the state-error covariance matrix $\tilde{\mathbf{R}}_c(k)$ compensates for numerical instability that is commonly encountered in Kalman filtering [38].

This article has been accepted for publication in a future issue of this journal, but has not been fully edited. Content may change prior to final publication. Citation information: DOI 10.1109/TWC.2020.3016962, IEEE Transactions on Wireless Communications

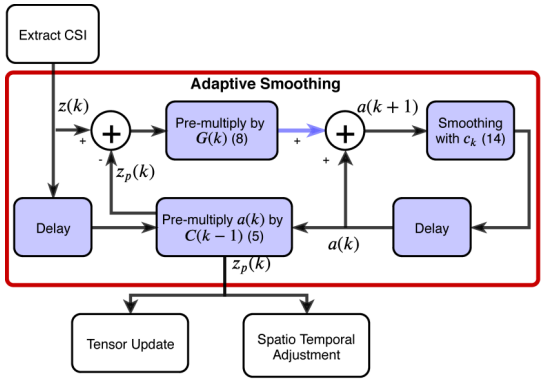

(a) Adaptive Smoothing system model

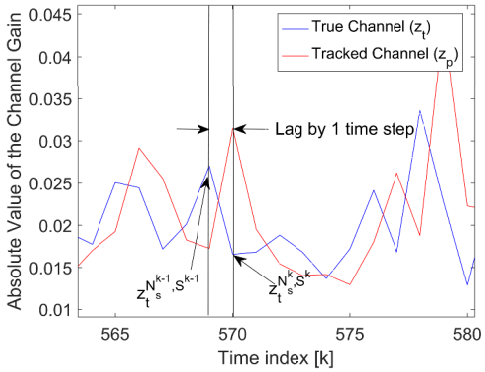

(b) The tracked channel lags the true channel.

Figure 4: Adaptive Smoothing System: In (a) corresponding equations are indicated in parenthesis

From (10), the tracked channel state, $\mathbf{z}_p(k)$ is defined in (13),

$$\mathbf{z}_p(k) = \mathbf{C}(k-1)\mathbf{a}(k) \tag{13}$$

which is formed by a weighted sum of the previous p measurement channel-state vectors as in (2). Figure 4a shows the Adaptive Smoothing system including the Kalman filter.

Additional Smoothing Step: The Kalman-AR combination is an iterative algorithm that is designed to converge on the last observed CSI. Therefore an inherent drawback of such a scheme is the lag in the tracked channel due to one time-step delay in the CSI feedback path. This phenomenon is shown in figure 4b. Evidently, $\mathbf{z}_p(k)$ (13) strives to converge to $\mathbf{z}_t(k-1)$ (the true channel at time $k-1$), because the Kalman-AR combination has the effect of minimizing the noise process in the measurement channel. Hence, an additional smoothing step is employed to mitigate the effect of undesired transients in the received CSI.

- Smoothing step:

$$\mathbf{c}_k = (c(\mathbf{a}(k+1) - \mathbf{a}(k))^2)./(\mathbf{1} + c(\mathbf{a}(k+1) - \mathbf{a}(k))^2) \tag{14}$$

$$\mathbf{a}(k+1) = (\mathbf{1} - \mathbf{c}_k).\mathbf{a}(k) + \mathbf{c}_k.\mathbf{a}(k+1) \tag{15}$$

where, c is the smoothing constant, $\mathbf{c}_k$ is the smoothing coefficients vector (where each component $c_k \in \mathbf{c}_k$ is such that $c_k \in (0,1)$), "." denotes the element-wise operations and $\mathbf{1}$ is a vector with all ones.

This nonlinear recursive smoothing step is applied to each component of $\mathbf{a}(k)$. (15) defines a lowpass filter for each k, where the degree of smoothing increases with the disparity in true and tracked channel. Using (15), the tracked channel coefficients are computed as in (13) as $\mathbf{z}_p(k) = \mathbf{C}(k-1)\mathbf{a}(k)$.

Limitations in Feedback-based Iterative tracking systems: Feedback-based iterative tracking systems rely only on the previous feedback of the CSI to track the temporal evolution of the channel and smooth the non-stationary noise in the CSI. A drawback of such systems is the inability to track the ephemeral transients in the channel statistics due to the tendency for the tracked channel to converge to a previous, stale channel state. This is shown in figure 4b. The inability to predict the current channel due to the dependence on previous CSI and lag in feedback is detrimental for higher order modulations like 64-QAM, which are highly susceptible to phase noise. Although the smoothing step introduced above helps in minimizing the effect of sudden and large changes in channel gain, it is still not accurate enough to maintain low error vector magnitude (EVM) for higher order modulations (as shown in Section V-B). The non-stationary ephemeral transients in the channel statistics can be attributed to certain changes in the observable parameters (such as the scattering environment and receiver location, as shown in figure 4b) which in turn can be tracked to account for the non-stationarity of the channel. The tensor factorization & completion framework (explained in Section IV-B) analyzes the effect of these measurable parameters on the CSI, and uses the impending parameters to predict the non-stationary transients in channel statistics. Hence, while the adaptive smoother tracks the long term evolution of the channel statistics, the tensor factorization & completion tracks the short lived changes in the channel statistics by observing the changes in the measurable parameters. Therefore, the output of the adaptive smoothing system as in (13) and as shown in figure 4a is adjusted to account for the spatio-temporal variations of the channel statistics as explained in Section IV-C.

B. Tensor Completion & Factorization

There is a disconnect between the tracked channel and the actual channel (as shown in figure 4b), which depends on the current scattering environment and location of the receiver. This information is embedded in the CSI, which consequently captures the deviation due to the change in the scatterers and the receiver location. We construct a 3D tensor shown in figure 5a to capture this property. The purpose of the tensor is to record these deviations and use them to make adjustments (details in Section IV-C) to the tracked channel, $\mathbf{z}_p(k)$. The measurement channel, $\mathbf{z}(k)$ derived from the CSI (see Section IV-D) is recorded in the tensor corresponding to the change in the observable parameters (change in scatterers (N_s^{k-1}, N_s^k) and segments (S^{k-1}, S^k)) over the time interval $[k-1, k]$. This represents a tube containing 100 pre-computed quantization levels (q). The output of the adaptive smoother, $\mathbf{z}_p(k)$ is quantized to the nearest level and the corresponding cell is populated with the measurement channel, $\mathbf{z}(k)$. This value is a running average of all $\mathbf{z}(k)$ that are mapped to that particular cell. Therefore, in essence, each cell contains the historical

This article has been accepted for publication in a future issue of this journal, but has not been fully edited. Content may change prior to final publication. Citation information: DOI 10.1109/TWC.2020.3016962, IEEE Transactions on Wireless Communications

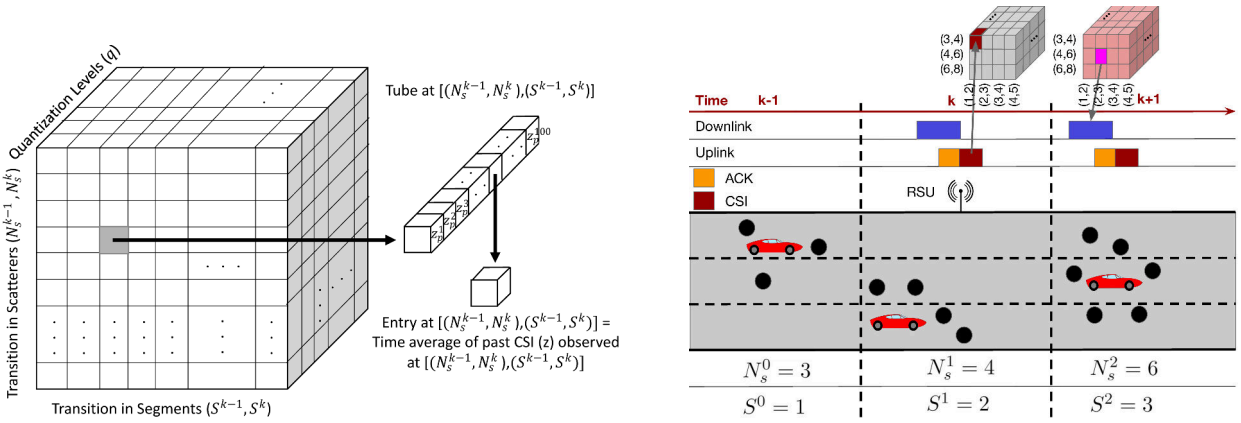

(a) Illustration of channel tensor $\mathcal{Z}$ and its entries. (b) Prediction life-cycle

Figure 5: Channel Tensor Update: At each time step k, $\mathcal{Z}$ is updated with the measurement channel, $\mathbf{z}(k)$ at the entry corresponding to the observed change in the measurable parameters.

CSI that is mapped to that quantization level q, observed for a given change in N_s and S. Figure 5b shows an example of V2X channel prediction, where the piggy-backed CSI is quantized and updated in one of the cells (q) in the tube $[(3,4),(1,2)]$ corresponding to the observed change in N_s and S at time (k). The quantized levels capture information required to update the predicted channel as in Sections IV-B2 and IV-C.

The channel in (1) contains many immeasurable and hidden variables that collectively contribute to a particular CSI value. However, these hidden variables may be correlated with observable parameters like the number of scatterers, vehicle location, vehicle speed and road-side features. Moreover, the key challenges in this tensor-based procedure are, sparsity (due to the large size of the tensor detailed in Section V and infrequent entries (CSI) that may not be observed over long duration of time), and noisy data in the tensor (due to noise in the CSI and incomplete filling of cells). These result in missing or corrupt adjustments. Hence, to account for these factors and extract an accurate representation of the channel based on the impending states of observable variables, we introduce the tensor factorization & completion approach. Tensor factorization is used to decompose the channel tensor into its constituent latent variables, in order to analyze the effect on the measured CSI by the observable parameters. Tensor completion generates accurate channel recommendations by recreating the missing entries of the channel tensor from these latent variables.

Thus, at each time step k, the channel tensor is updated with the measurement channel, $\mathbf{z}(k)$. This channel tensor is factorized (Section IV-B1) into a factor model to capture the latent structure of the underlying process under sparse conditions. The tensor is reconstructed using the factorized model (Section IV-B2) to extract missing entries. The completed tensor is used to generate recommendations, $\mathbf{z}_r(k)$ which is used to adjust the tracked channel, $\mathbf{z}_p(k)$ (Section IV-C) corresponding to the location of a target vehicle and the scattering environment. For example, in figure 5b, after tensor factorization and completion, the recommended downlink channel is obtained from the cell corresponding to the impending change in N_s and S in time-step $(k+1)$, i.e., $[(4,6),(2,3)]$. In this way, predictions can be made even for cells that are sparse and the values reflect the cumulative contribution of the latent factors that are buried in the CSI.

1) Tensor Factorization: Tensor factorization is employed to capture latent structure of the channel tensor by expressing it as the sum of component rank-one tensors [39]. This latent structure is used to reconstruct missing entries in the tensor in Section IV-B2. Figure 6 shows the tensor factorization of the third order channel tensor.

Here, scalars are denoted by lowercase letters (e.g., a), vectors by boldface lowercase letters (e.g., $\mathbf{a}$), matrices by boldface capital letters (e.g., $\mathbf{A}$), higher-order tensors by boldface Euler script letters (e.g., $\mathcal{Z}$). The i^{th} entry of a vector $\mathbf{a}$ is denoted by a_i, element (i,j) of a matrix $\mathbf{A}$ is denoted by a_{ij}, and element (i,j,k) of a third-order tensor $\mathcal{Z}$ is denoted by z_{ijk}. The j^{th} column of a matrix $\mathbf{A}$ is denoted by $\mathbf{a}_j$. The n^{th} element in a sequence is denoted by a superscript in parentheses, e.g., $\mathbf{A}^{(n)}$ denotes the n^{th} matrix in a sequence. Let $\mathcal{Z}$ be the three-way channel tensor of rank R and size $I \times J \times K$. Then the channel tensor decomposition is defined by factor matrices $\mathbf{A}$, $\mathbf{B}$, and $\mathbf{C}$ of sizes $I \times R$, $J \times R$, and $K \times R$ (defined in figure 6) that minimize the objective function in (16),

$$f_{\mathcal{W}}(A,B,C) = \underbrace{\frac{1}{2}\sum_{i=1}^{I}\sum_{j=1}^{J}\sum_{k=1}^{K}\left\{w_{ijk}\left\{z_{ijk} - \sum_{r=1}^{R} a_{ir}b_{jr}c_{kr}\right\}\right\}^2}_{\text{Error function}} + \underbrace{\frac{\lambda}{2}\sum_{r=1}^{R}\left\{\sum_{i=1}^{I}||a_{ir}||^2 + \sum_{j=1}^{J}||b_{jr}||^2 + \sum_{k=1}^{K}||c_{kr}||^2\right\}}_{\text{Regularization term}} \tag{16}$$

The *error function* is employed to account for CSI noise in the channel tensor (i.e., imperfect data) and the weighted version of the error function is used to address sparsity by ignoring missing data and modeling only the known entries [30]. Consequently, minimizing the above objective function ensures that the recommendations, $\mathbf{z}_r(k)$ accurately represents

This article has been accepted for publication in a future issue of this journal, but has not been fully edited. Content may change prior to final publication. Citation information: DOI 10.1109/TWC.2020.3016962, IEEE Transactions on Wireless Communications

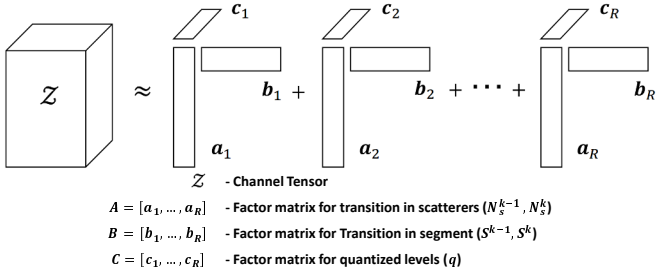

Figure 6: Channel tensor factorization for third-order tensor. $\mathbf{A}=[\mathbf{a}_1, \ldots, \mathbf{a}_R]$, $\mathbf{B}=[\mathbf{b}_1, \ldots, \mathbf{b}_R]$, $\mathbf{C}=[\mathbf{c}_1, \ldots, \mathbf{c}_R]$ are the factor matrices for transition in number of mobile scatterers, transition in segments and quantized levels respectively.

the discrepancy in channel tracking, even in the case of missing entries. Here, $\mathcal{W}$ denotes a nonnegative weight tensor (representing the sparsity of the channel tensor $\mathcal{Z}$), with entries of '1', when z_{ijk} is known and entries of '0', when z_{ijk} is missing, for all $i = 1, \ldots, I, j = 1, \ldots, J, k = 1, \ldots, K$. The *regularization term* penalizes the size of the latent factors and consequently avoids over-fitting the noise in the measurement channel, $\mathbf{z}(k)$ and ensures the generality of the tensor, $\mathcal{Z}$ over space and time. The regularization parameter, λ is a nonnegative value that balances the modeling error and the complexity of the latent structure. For convenience the objective function in (16) is expressed in (17) as,

$$f_{\mathcal{W}}(\mathbf{A}, \mathbf{B}, \mathbf{C}) = \frac{1}{2}||\mathcal{Z} - [\![\mathbf{A}, \mathbf{B}, \mathbf{C}]\!]||^2_{\mathcal{W}} + \frac{\lambda}{2}(||\mathbf{A}||^2 + ||\mathbf{B}||^2 + ||\mathbf{C}||^2) \tag{17}$$

$$\text{where,} \quad [\![\mathbf{A}, \mathbf{B}, \mathbf{C}]\!] = \sum_{r=1}^{R} \mathbf{a}_r \circ \mathbf{b}_r \circ \mathbf{c}_r$$

Here $[\![\cdot]\!]$ represents the Kruskal operator shorthand notation [39], '$\circ$' refers to the outer product, $||\cdot||$ refers to the analogous Frobenius and two-norm for matrices and vectors respectively, while $\|\mathcal{Z}\|_{\mathcal{W}}$ is the W-weighted norm of $\mathcal{Z}$, defined as $\|\mathcal{Z}\|_{\mathcal{W}} = \|\mathcal{W} \odot \mathcal{Z}\|$. Here '$\odot$' represents the Hadamard (elementwise) product of tensors. The objective function in (17) is minimized by a nonlinear gradient-based optimization [30], to find the latent factor matrices $\mathbf{A}, \mathbf{B}, \mathbf{C}$.

2) Tensor Completion: This stage, reconstructs the tensor $\hat{\mathcal{Z}}$ (Recommendation tensor) from the computed factorization model $(\mathbf{A}, \mathbf{B}, \mathbf{C})$ in (17) by filling in the missing entries of tensor $\mathcal{Z}$ and is given by (18),

$$\hat{\mathcal{Z}} = \mathcal{W} \odot \mathcal{Z} + (\mathbf{1} - \mathcal{W}) \odot [\![\mathbf{A}, \mathbf{B}, \mathbf{C}]\!] \tag{18}$$

where $\mathbf{1}$ is the tensor of all ones and is the same size as $\mathcal{Z}$. Recent work [40] shows that even if a small amount of entries (CSI) are available and those are corrupted with noise, it is still possible to recover the missing entries up to the level of noise. The recommendation tensor, $\hat{\mathcal{Z}}$ is used to obtain the recommendations, $\mathbf{z}_r(k)$ corresponding to the tracked channel, $\mathbf{z}_p(k)$. These are the N entries of tensor $\hat{\mathcal{Z}}$ at indices corresponding to, transitions for number of scatterers, $[N_s^{k-1}, N_s^k]$ and segment number, $[S^{k-1}, S^k]$ from the last observed CSI, and the quantized levels corresponding to the tracked channel, $\mathbf{z}_p(k)$. Let the tracked channel for N subcarriers be, $\mathbf{z}_p(k) = [z_p(k,1), z_p(k,2) \ldots z_p(k,N)]^T$. Hence, at each iteration N recommendations $(z_r(k,n))$ are made as in (19),

$$z_r(k,n) = \hat{\mathcal{Z}}[(N_s^{k-1}, N_s^k), (S^{k-1}, S^k), q_n] \quad \forall n = 1, \ldots, N \tag{19}$$

Here, $\hat{\mathcal{Z}}[(N_s^{k-1}, N_s^k), (S^{k-1}, S^k), q_n)]$ is the entry of $\hat{\mathcal{Z}}$ at index $[(N_s^{k-1}, N_s^k), (S^{k-1}, S^k), q_n]$ as in figure 5a and q_n is the quantization level of $z_p(k,n)$. Then the recommended channel for N subcarriers, $\mathbf{z}_r(k)$ is given by (20),

$$\mathbf{z}_r(k) = \begin{bmatrix} z_r(k,1) & z_r(k,2) \ldots & z_r(k,N) \end{bmatrix}^T \tag{20}$$

C. Spatio-Temporal Adjustment

At each time step k, the tracked channel $\mathbf{z}_p(k)$ is improved to $\hat{\mathbf{z}}_p(k)$ (predicted channel) by incorporating the recommendations, $\mathbf{z}_r(k)$ from (20) using a normalized weighted average:

$$\begin{aligned} \hat{\mathbf{z}}_p(k) &= (1 - \alpha_k)\mathbf{z}_p(k) + \alpha_k \mathbf{z}_r(k)) \\ &= \mathbf{z}_p(k) + \alpha_k(\mathbf{z}_r(k) - \mathbf{z}_p(k)) = \mathbf{z}_p(k) + \alpha_k \delta \mathbf{z}_p(k) \end{aligned} \tag{21}$$

where α_k is the normalization weight at time step k (a design parameter assuming a value between 0 and 1). This has the effect of updating the tracked channel, $\mathbf{z}_p(k)$ by a delta adjustment of the form $\delta \mathbf{z}_p(k) = \mathbf{z}_r(k) - \mathbf{z}_p(k)$. A channel adjustment of this form alleviates the lag and the disparity in the channel states due to the change in the measurable parameters (N_s and S). Since, the tracked channel is adjusted with the recommendations based on the observable parameters (scattering environment and the location of the target vehicle), the predicted channel, $\hat{\mathbf{z}}_p(k)$ is able to account for the non-stationarity of the actual channel over time, space and vehicle density.

D. Pre-equalization at Transmitter

In order to take advantage of the predicted channel profile, the waveform of the downlink packet is pre-equalized such that when convolved with the true channel, the net effect is a flat fading at the receiver, that can be easily equalized using pilot based linear interpolation methods commonly used in OFDM communication. This method of channel inversion has been used to compensate channel impairments largely because of simple arithmetic computations [13] and since, it eliminates any complex, power inefficient processing algorithms [14] at the receiver. The pre-equalized channel, $\tilde{\mathbf{z}}_p(k)$ is given by (22),

$$\tilde{\mathbf{z}}_p(k) = \mathbf{1}./\hat{\mathbf{z}}_p(k) \tag{22}$$

Conceptually, $\tilde{\mathbf{z}}_p(k)$ represents the inverse of the expected fading profile of the true channel, $\mathbf{z}_t(k)$ (details in Section V-A). Hence, the resultant channel, $\mathbf{z}_f(k)$, as estimated by the receiver vehicle is given by Hadamard product ($\odot$, which is equivalent to convolution in time-domain),

$$\mathbf{z}_f(k) = \mathbf{z}_t(k) \odot \tilde{\mathbf{z}}_p(k) + \mathbf{w}(k) \tag{23}$$

where, $\mathbf{w}(k)$ is an additive term that captures the effect of the noise and estimation errors. The CSI, $\mathbf{z}_f(k)$, captures the interaction between the true channel $\mathbf{z}_t(k)$ and the pre-equalized channel $\tilde{\mathbf{z}}_p(k)$, and is fed back to the transmitter. At

This article has been accepted for publication in a future issue of this journal, but has not been fully edited. Content may change prior to final publication. Citation information: DOI 10.1109/TWC.2020.3016962, IEEE Transactions on Wireless Communications

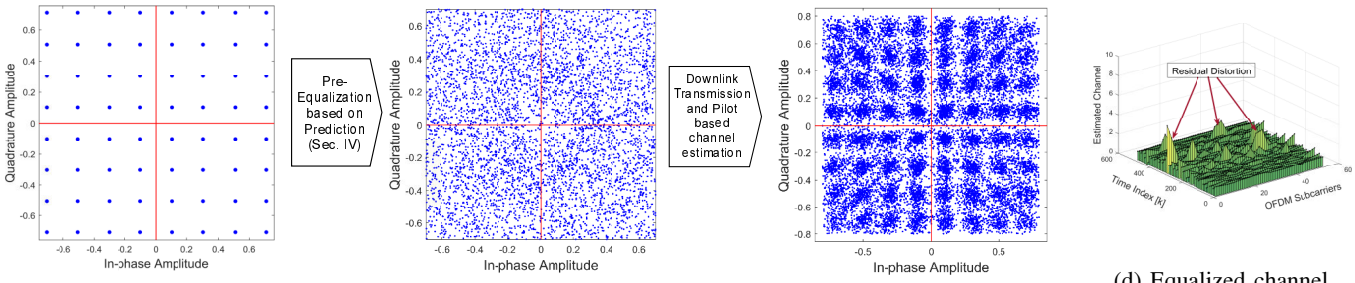

(a) Before compensation (b) After Pre-equalize (c) Received constellation (d) Equalized channel

Figure 7: High level system performance: a) The constellation for ideal 64-QAM symbols used for downlink transmission. b) The ideal I/Q vectors are pre-equalized with the predicted channel profile $\tilde{\mathbf{z}}_p(k)$. c) The received symbol constellations using linear interpolation equalizer. d) The equalized channel in time and frequency domain at the receiver. The estimated channel is largely flat that achieves low BER (details in Section V).

the transmitter, the measurement channel $\mathbf{z}(k)$ is computed, by combining (21) and (23),

$$\begin{aligned}\mathbf{z}(k) &= \mathbf{z}_f(k) \odot \hat{\mathbf{z}}_p(k) + \mathbf{w}(k) \\ &= \mathbf{z}_f(k)./\tilde{\mathbf{z}}_p(k) + \mathbf{w}(k)\end{aligned} \tag{24}$$

Mathematically, $\mathbf{z}(k)$ represents the error in the recommendation along with added system and numerical noise in the feedback loop. This forms the new input to the recommender system described in Section IV-B. Figure 7 shows the constellation diagram for a packet with 64-QAM modulation. The ideal constellation in figure 7a is pre-equalized by changing the I/Q vectors in the modulator using the predicted channel, as shown in figure 7b. Figure 7c shows the clean equalized constellation at the receiver with the corresponding channel profile in figure 7d. These results show that the channel recommender system works very well for higher order constellations as well. However, there are cases when residual distortion remain at the receiver, but the penalty in BER for those cases are minimal.

Complexity of the Channel Recommender: The run-time complexity of the channel recommender at each prediction step is determined by the four stages outlined in Sections IV-A–IV-D. The complexity of adaptive smoothing (from (2)–(15)) is dominated by the matrix multiplications and inversion operations in (8) and is be computed in $O(N^{2.376})$ [41], where N is the number of frequency subcarriers. The time complexity of tensor decomposition using nonlinear gradient based optimization is $O(RIJK)$ [42], where R is the rank and I, J, K are the number of rows of the factor matrices $\mathbf{A}, \mathbf{B}, \mathbf{C}$. Tensor completion involves the Hadamard product and addition of tensors and has a worst-case complexity of $O(RIJK)$. The spatio-temporal adjustment and pre-equalization stages involve vector operations, resulting in a complexity of $O(N)$. Hence, the overall complexity of the channel recommender at the transmitter is $O(N^{2.376}+2RIJK+N) \approx O(\max\{N^{2.376}, RIJK\})$. The values of N, R, I, J, K are preset as a design choice trading off the complexity and accuracy of channel tensor factorization & completion as explained in Section V-A. Hence, this demonstrates the low complexity of the prediction algorithm and its ability to be adapted in real-time.

V. Results

A. Simulation setup

We validate the efficacy of prediction and pre-equalization at the transmitter for non-stationary channels using V2X channels as an example. Figure 8 illustrates the emulated testbed to reflect a practical V2X network. The V2X channel is modeled using the WINNER channel toolbox in Matlab [43], which was used to generate 1000 channel instances for each segment (S) of the road. These channel instances are used to emulate a schedule of downlink transmissions (i.e., the true channel $\mathbf{z}_t$), by randomly selecting a segment at each time step and selecting the channel state for that segment. In reality, this schedule is not observed by the vehicles, but is used here to evaluate the accuracy and performance of the recommender system in terms of the mean squared error at the transmitter and the BER and EVM at the receiver. The WINNER channel toolbox has been shown to accurately reflect the real V2X channel using practical measurements in [44]. Moreover, this simulated test-bed gives the freedom to address a variety of different scenarios of non-stationary channels channel and propagation environments that may not be observed without extensive measurement campaigns. The parameters for the evaluation are as follows. The AR-model order is 3 (which empirically yields the best Kalman-AR tracking), and target vehicle's speed is V=20 m/s (45 mph). The target vehicle's and the transmitter's antenna heights are 1.5m and 2.5m respectively, from the surface of the road. The transmitter is placed at the center of the road and it is assumed that there is a Line-of-Sight (LOS) propagation and the transmitter-vehicle communication link is not intercepted by large vehicles. According to Intelligent Transportation System Joint Program Office, in connected vehicle (CV) technology, it is mandated that each vehicle will continually transmit their position, direction, and speed, to other vehicles and roadside units in the neighbourhood [45], [46]. This information can be used by the transmitter (e.g., RSU) to determine the receiver location and calculate the number of mobile scatterers in the vicinity of the receiver. The overall feasibility of the CV framework has been studied and methods to limit the communication overhead are demonstrated in [47].

This article has been accepted for publication in a future issue of this journal, but has not been fully edited. Content may change prior to final publication. Citation information: DOI 10.1109/TWC.2020.3016962, IEEE Transactions on Wireless Communications

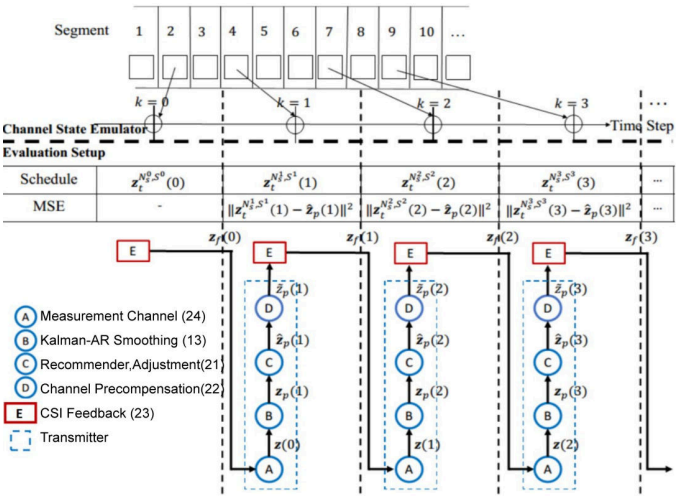

Figure 8: Measurement channel life-cycle: Relationship between true, measurement, smoothed, predicted and compensated channels. Corresponding equations are shown in parenthesis.

The number of fixed scatterers (deterministic road-side features) is different in each segment (between 1 to 5). The number of variable scatterers is modeled as a uniform random variable between 0 and 9. Consequently, the possible transitions, $[N_s^{k-1}, N_s^k]$, form a (10×10)×1=100×1 array. The road length is set to d_{road}=200 m and divided into 20 segments (i.e. d_{seg}=10 m) and the possible transitions in segment number, $[S^{k-1}, S^k]$, form a (20×20)×1=400×1 array. The number of quantization levels for the tracked channel $\mathbf{z}_p$ (determined by the trade-off of accuracy and computational cost of the recommender) is limited to 100, forming a 100×1 array. This data is used to construct the channel tensor $\mathcal{Z}$ of size 100×400×100. The tensor factorization rank [30] was empirically determined to be R=3, which yielded the least prediction error for the recommender.

B. BER & EVM at the Receiver

Figures 9a, 9b and 9c show the BER performance corresponding to an OFDM packet of 100 random bits using different modulation and coding at a carrier frequency of f_c=5.9GHz and sampling frequency of f_s=10MHz. Figure 9a shows the BER performance for 16-QAM modulation and 1/2 coding, with and without (as in conventional 802.11p) channel recommendation, with pilot-based linear interpolation equalization employed at the receiver. The frequency selective fading of V2X channel is very well compensated (shown in figure 7d) resulting in a BER improvement by 90%, which is very encouraging. In contrast, conventional receiver algorithms are simply not sufficient to track the channel over space, time and frequency, hence performing much worse even at high SNR. This is another motivating reason to adopt a channel recommender at the transmitter. The ideal scenario represents an oracle with complete knowledge of channel properties, which is shown for comparison. The channel recommender requires only 8dB more SNR to achieve the same BER as the ideal case as highlighted in figure 9a. The figure also emphasizes the 79% improvement in BER (at 20dB SNR) over adaptive smoothing techniques, by incorporating tensor-based channel recommendations in Sections IV-B and IV-C. This confirms the efficacy of the proposed channel recommender for non-stationary channel prediction, over conventional channel prediction approaches based on feedback based iterative tracking (such as Kalman Filtering). Figure 9b shows the BER performance for different modulation schemes and the ability of the algorithm to support higher order modulation schemes (like 64-QAM) with low BER. Figure 9c emphasizes the improvement in the BER for higher order modulations by incorporating more pilot subcarriers. The non-stationary channel has a low coherence bandwidth and changes every 5 subcarriers (explained in Section V-E) for the PHY parameters of 802.11p. Thus, 16 pilot subcarriers (3 subcarrier spacing) can sufficiently track the frequency domain channel impairments, while the use of 4 pilots (14 subcarrier spacing) cannot.

Figures 9d and 9e show the EVM performance of the channel recommender. Figure 9d shows the EVM performance for different modulation schemes, with and without channel recommendation. It shows an almost ideal performance of the EVM up to 16dB SNR, which is very encouraging. Figure 9e confirms the improvement in EVM with the number of pilots.

C. Throughput-Pilot Trade-off

In 802.11p, four pilot tones are inserted in subcarriers [-21 -7 7 21] and are used to estimate the channel. While incorporating more pilot tones, improves the channel estimation at the receiver and results in a lower BER & EVM performance and more accurate prediction of the channel (as shown in figures 9c and 9e), it reduces the theoretical throughput, since the number of active tones is less. Figure 9f shows that while the transmission throughput reduces with increasing number of pilots, the drop in the *achievable* throughput is relatively less, since the BER also decreases. Hence, we can choose higher order modulations for V2X transmission to achieve higher throughput, while maintaining the same BER. For instance, a 64-QAM scheme with 16 pilots has similar BER performance as a 16-QAM scheme with 4 pilot tones while providing higher data rate. Figure 9f also emphasizes that the recommender with a 4 pilot tone channel estimation, is sufficient to provide good BER performance and clean constellations for BPSK and QPSK and that more dense constellations require more pilots to achieve comparable BER performance due to their low margin of error (as seen in figure 7c). Using more pilots is justified for higher order modulations as they offer higher throughput compared to BPSK and QPSK.

D. Impact of Speed of vehicles and Lanes on the BER

The higher the *relative speed* between the transmitter and receiver, the higher is the Doppler shift and the lower is the coherence time and coherence frequency (explained in Section V-E) of the non-stationary channel. Consequently, the channel statistics vary rapidly, making it more challenging to track the channel and negatively impacts the BER at the receiver. Unlike in Vehicle-to-Infrastructure (V2I) channels where only the receiver is mobile, in Vehicle-to-Vehicle (V2V) channels it

This article has been accepted for publication in a future issue of this journal, but has not been fully edited. Content may change prior to final publication. Citation information: DOI 10.1109/TWC.2020.3016962, IEEE Transactions on Wireless Communications

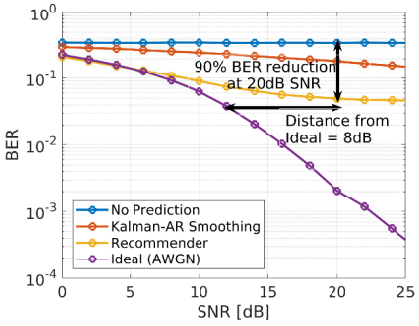

(a) BER for 16-QAM with 16 pilot tones.

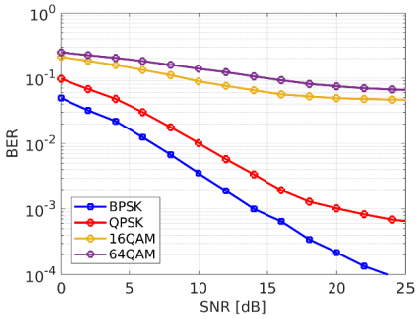

(b) BER for different modulation with 16 pilot tones.

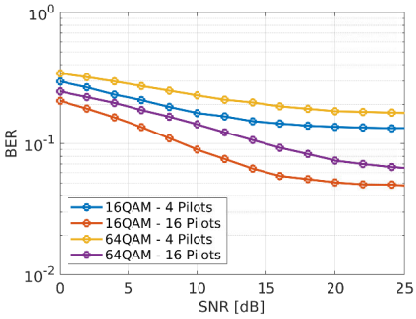

(c) BER for 16QAM and 64QAM with varying pilot tones

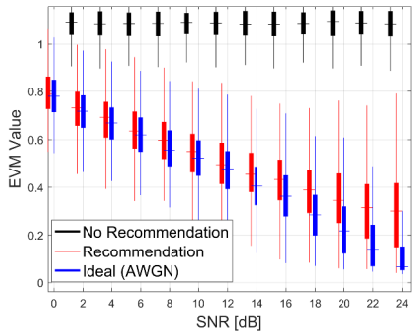

(d) EVM distribution for 16QAM with 16 pilot tones

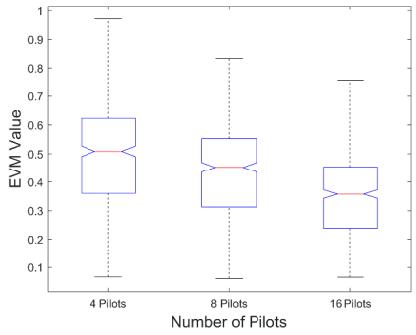

(e) EVM plot for 16QAM with varying pilot tones at 20dB SNR.

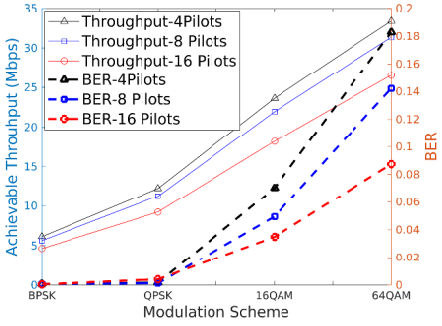

(f) Throughput and BER for different modulation and pilots.

Figure 9: Performance of Recommendation system at the Receiver. The BER is almost *two orders of magnitude* lower than conventional methods used in 802.11p. Also, it requires only 8dB more SNR to achieve the same BER as the ideal case (perfect estimation).

is the relative speed of the transmitting and receiving vehicles that impacts the channel coherence. The impact on the BER due to the speed of the receiving vehicle is shown in figure 10a, with pilot-based linear interpolation equalization employed at the receiver. It is observed that the quality of the transmission degrades as the speed of the receiver increases. The speed of the receiving vehicle is reflected in the variation in the road segment in which the vehicle is located. For example, a vehicle traveling at 20 m/s, translates through two road segments in the same direction in 1 second, while a vehicle traveling at 40 m/s, translates through four segments. Since the recommender learns the impact of the change in the location of the receiving vehicle on the channel statistics (explained in Section IV-B), it is capable of predicting the channel profile regardless of the speed of the receiving vehicle. The BER for a receiver traveling at 67 mph is only 8% more than the BER at a receiver speed of 45 mph, and the BER when the receiver is traveling at 89 mph is about 20% more. This shows the ability to use higher order modulations even for highly mobile communicating entities by employing predictive analytics at the transmitter.

Typically rural streets have one lane, suburban and urban streets have one to two lanes while highways have two to six lanes in each direction [15]. To study the impact of multiple lanes on the fidelity of communications, 1000 channel instances were generated for each segment and each lane of the road using the WINNER channel toolbox. The downlink transmissions to different vehicles at different lanes and segments were emulated by, randomly selecting a segment and lane at each time step and selecting the channel state for that segment and lane. Figure 10b compares the BER performance at the receiver, for three streets consisting of different number of lanes, with pilot-based linear interpolation equalization at the receiver. In the presence of multiple lanes, the possibility of increased traffic density, considerably increases the variation in the scatterer distribution within the same road segment and the possibility of dominant multi paths. However, the recommender learns the impact on the channel statistics for different scatterer distributions and consequently mitigates the negative impact on the BER at the receiver. The BER performance is similar for low and moderate SNR for the streets with a single lane, two lanes or four lanes. However at a high SNR of 20dB we observed a 20% increase in the BER at the receiver, on a highway with 4 lanes when compared to a single lane street.

E. Comparison with Receiver-side Equalization techniques

Limitations of Receiver-side Equalization techniques: The frequency selectivity of non-stationary channels like the V2X channel poses a great challenge for broadband communication using frequency domain modulation such as OFDM. Furthermore, the standards advocated for WAVE [9] are based on Dedicated Short Range Communication (DSRC) messages that are not robust enough to compensate for the rich fading environment [14]. These waveforms preserve much of the PHY and MAC layer parameters from the 802.11a/g [48].

This article has been accepted for publication in a future issue of this journal, but has not been fully edited. Content may change prior to final publication. Citation information: DOI 10.1109/TWC.2020.3016962, IEEE Transactions on Wireless Communications

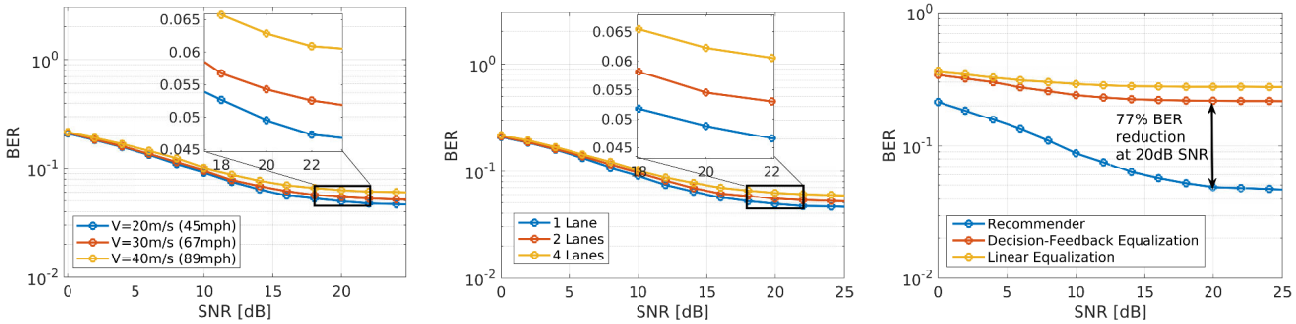

(a) BER for varying speeds of the communicating vehicles

(b) BER for different streets with different numbers of lanes.

(c) BER comparison with state-of-the-art receiver side techniques

Figure 10: BER performance of the Recommender system for a 16-QAM modulation with 1/2 coding: a) with varying vehicle speeds, b) for streets with different number of lanes, and c) comparison with state-of-the-art receiver-side techniques.

Now, assuming a vehicle is moving at 50 mph or 22 meters/sec, the maximum Doppler shift is, $f_D^{max}=v/\lambda_c=438Hz$, for a center frequency of 5.9 GHz. Therefore, the channel coherence time, which provides a measure of how fast the channel is changing over time, is, $T_{coh}=1/(2\pi f_d)\approx 363\mu s$; With the PHY parameters of 802.11p, the coherence time (T_{coh}) translates to 43 OFDM symbols ($8\mu s$/symbol). If we assume that the channel condition can support QPSK-3/4 modulation and coding (or 18 Mbps), which allows 72 uncoded data bits per OFDM symbol, a 1KB payload will require 85 symbols. Therefore, the *coherence time of a typical 802.11p channel is even* ***less*** *than the transmission time of a 1KB packet*. Furthermore, the coherence bandwidth B_{coh}, which is a measure of channel impairment in frequency domain, is expressed as, $B_{coh}=1/(2\pi\tau_{rms})=800KHz$, assuming, $\tau_{rms}=2T_s=200ns$, where T_s is the sample time [33]. Now, $800KHz$ spans $B_{coh}/\Delta f\approx 5$ subcarriers ($\Delta f=$ subcarrier spacing in 802.11p is 156.25KHz), which means that in frequency domain the channel changes every 5 subcarriers, while the pilot spacing in conventional 802.11p is 14. In other words, *the channel changes at a faster rate than the frequency of occurrence of the pilot subcarriers and hence the pilots are* ***unable*** *to track the channel in frequency domain*.

Pilot based channel estimation and equalization employed in OFDM receiver performs best if the fading profile between the pilot subcarriers is mostly flat or at least linear [49]. Hence, conventional pilot based channel estimation are not sufficient to combat nonstationary channel inefficiencies as discussed in Section V-B. Linear equalization techniques such as the Zero Forcing (ZF) equalizer and the Minimum Mean-Squared Error (MMSE) equalizer are easy to implement, however typically suffer from noise enhancement at the receiver and perform well when the channel is linear. Non-linear methods like Decision Feedback Equalization (DFE) [24], [25] and Maximum Likelihood Sequence Estimation (MLSE) add complexity that are unsuitable for hardware implementation and adds considerable processing latency at the receiver. DFE equalization has been employed to track the vehicular channel in [50], [25], due to it's relatively better ability to track the channel's impulse response compared to linear equalizers. However on channels with low SNR, the DFE suffers from error propagation. While MLSE is an optimal equalization technique, the fact that it's complexity grows exponentially with the length of the delay spread [51], makes it unsuitable for non-stationary channels such as V2X channels which have a large delay spread. Figure 10c compares the BER performance of the receiver-side linear MMSE equalizer and the DFE equalizer with the pre-equalization from the recommender at the transmitter. Even though DFE outperforms the linear equalizer, it is not sufficient to track the non-stationarity of the channel. The figure demonstrates a 77% improvement in the BER performance by employing proactive pre-equalization at the transmitter based on the predicted channel, compared to the complex receiver-side DFE equalizer.

F. Performance of the Recommender System at the Transmitter

Figure 11a shows the Tensor Completion Score (TCS) which represents the relative error in the missing entries as defined in [30] (TCS is always nonnegative and the best possible score is 0). As more CSI is received as feedback from the vehicles, more entries are recorded in the tensor and the tensor becomes less sparse. Hence, the recommender is able to reconstruct missing entries more accurately and the TCS improves over time, and consequently results in more accurate channel predictions. The figure also shows the effectiveness of the tensor completion approach (explained in Section IV-B2) in reconstructing the missing recommendations even in the presence of few CSI. Figures 11b & 11c show the accuracy of the channel recommender, in terms of the Mean Squared Error (MSE) between the predicted channel coefficients and the true channel as generated in Section V-A (shown in figure 8), over 1000 channel instances. Figure 11b shows that the variance about the median error and the median value of the MSE is stationary across the frequency subcarriers, and confirms that the recommendation algorithm is able to track the non-stationary channel with high accuracy. Figure 11c shows the reduction in MSE over time and the improvement in channel recommendation. It is evident that with time, as more entries are recorded, the MSE reduces since the sparsity and noise in the tensor reduces, leading to an improvement in accuracy of the channel recommender with time.

This article has been accepted for publication in a future issue of this journal, but has not been fully edited. Content may change prior to final publication. Citation information: DOI 10.1109/TWC.2020.3016962, IEEE Transactions on Wireless Communications

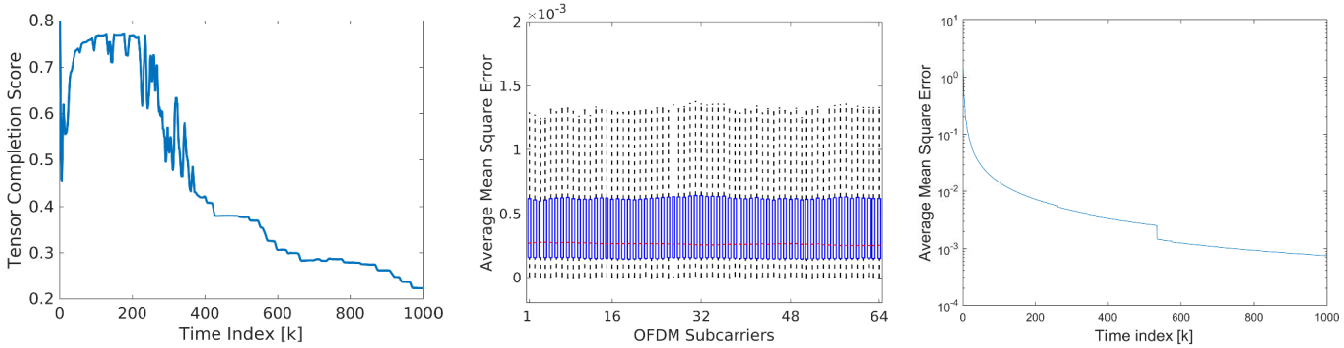

(a) Tensor Completion Score improves with more CSI entries in the tensor.

(b) Mean squared error is stationary for each frequency subcarrier

(c) Mean squared error reduces with more CSI entries in the tensor.

Figure 11: Performance of predictive analytics at the transmitter. a) Tensor Completion Score improves with more CSI entries in the tensor, b) The statistics of mean squared error are stationary across the OFDM subcarriers, which shows accurate tracking by the prediction algorithm, c) The reduction in mean squared error over time shows the improvement in predictions with time.

VI. Generalized Framework for any Non-Stationary Channel

The design of the V2X channel recommender system, in this work, considers the information about the scatterer density and the location of the target receiver as the measurable parameters to make channel predictions. This technique can be used to predict the channel profile for any *generic non-stationary channel* by considering the set of available measurable parameters. For example, in addition to the scattering environment and receiver location, the antenna configuration (the polarization, directivity and number of antenna elements) for Massive MIMO and mmWave communication, and the transmitter location for V2V communication are measurable parameters that affect the channel statistics. Let $\mathfrak{M} = \{\mathcal{M}_1, \mathcal{M}_2, \ldots, \mathcal{M}_N\}$ denote the set of N such measurable parameters. A brief sketch of the steps required to make real time channel predictions of any non-stationary channel using the channel recommender system is provided below. To address the generalized non-stationary channel prediction problem the channel tensor factorization in (17) is extended to an N-dimensional tensor $\mathcal{Z}$ (N-way tensor) factorization, giving way to the N-way objective function defined by,

$$f_{\mathcal{W}}(\mathbf{A}^{(1)}, \ldots, \mathbf{A}^{(N)}) = \frac{1}{2}\left\|\mathcal{Z} - [\![\mathbf{A}^{(1)}, \ldots, \mathbf{A}^{(N)}]\!]\right\|^2_{\mathcal{W}} + \frac{\lambda}{2}\sum_{n=1}^{N}||\mathbf{A}^{(n)}||^2 \qquad (25)$$

where $[\![\mathbf{A}^{(1)}, \ldots, \mathbf{A}^{(N)}]\!] = \sum_{r=1}^{R} \mathbf{a}_r^n \circ \ldots \circ \mathbf{a}_r^n$, and the factor matrices are defined as $\mathbf{A}^{(n)} = [\mathbf{a}_1^N, \ldots, \mathbf{a}_R^N]$, with size $I_n \times R$, for $n = 1, \ldots, N$, where $\mathbf{A}^{(1)}, \ldots, \mathbf{A}^{(N)}$ are the latent factor matrices corresponding to the transition in the measurable parameters, $\mathcal{M}_1, \mathcal{M}_2, \ldots, \mathcal{M}_N$ respectively. The objective function in (25) is minimized using the method outlined in Section IV-B. Tensor completion is then used to construct the recommendation tensor as, $\hat{\mathcal{Z}} = \mathcal{W} \odot \mathcal{Z} + (\mathbf{1} - \mathcal{W}) \odot [\![\mathbf{A}^{(1)}, \ldots, \mathbf{A}^{(N)}]\!]$ and obtain the predicted channel, $\hat{\mathbf{z}}_p(k)$ similar to Sections IV-B and IV-C. The overall run-time complexity of the generalized predictive framework for any non-stationary channel is $O(\max\{N^{2.376}, R\prod_{n=1}^{N} I_n\})$, where the values of I_n for $n = 1, \ldots, N$ are predetermined, consequently leading to a fixed time-complexity. This shows the adaptability of the channel recommender approach to address any non-stationary propagation environment.

VII. Conclusion

In this work, we have shown the power of recommender systems in predicting channel profiles for highly dynamic non-stationary wireless environments, using V2X networks as an example. Through modelling, analysis and simulations, we draw three conclusions: 1) The channel recommender is able to successfully predict the spatio-temporal non-stationary channel to achieve an almost flat fading profile at the receiver and obtain 90% lower BER, 2) This enables higher modulation schemes to be used in non-stationary communications for high throughput, and 3) The accuracy of the recommender system improves with time asymptotically achieving an MSE of 10^{-3}. Therefore, the encouraging results from this work will form the core of robust and highly reliable communication over non-stationary channels, supporting demanding emerging mobile applications.

References

[1] J. Wu and P. Fan, "A survey on high mobility wireless communications: Challenges, opportunities and solutions," *IEEE Access*, vol. 4, pp. 450–476, 2016.

[2] P. Bisaglia, L. Sanguinetti, M. Morelli, N. Benvenuto, and S. Pupolin, "Pre-equalization Techniques for Downlink and Uplink TDD MC-CDMA Systems," *Wireless Personal Communications*, vol. 35, no. 1-2, pp. 3–18, oct 2005. [Online]. Available: http://link.springer.com/10.1007/s11277-005-8736-8

[3] F. Tufvesson, "Pre-Compensation for Rayleigh Fading Channels in Time Division Duplex OFDM Systems," 2001.

[4] Google Inc., "Google Self-Driving Car Project." [Online]. Available: http://www.google.com/selfdrivingcar/

[5] G. Karagiannis, O. Altintas, E. Ekici, G. Heijenk, B. Jarupan, K. Lin, and T. Weil, "Vehicular networking: A survey and tutorial on requirements, architectures, challenges, standards and solutions," *IEEE Communications Surveys and Tutorials*, vol. 13, no. 4, pp. 584–616, 2011.

[6] M. Boban, T. T. V. Vinhoza, M. Ferreira, J. Barros, and O. K. Tonguz, "Impact of vehicles as obstacles in Vehicular Ad Hoc Networks," *IEEE Journal on Selected Areas in Communications*, vol. 29, no. 1, pp. 15–28.

[7] M. Boban, J. Barros, and O. K. Tonguz, "Geometry-Based Vehicle-to-Vehicle Channel Modeling for Large-Scale Simulation," vol. 63, no. 9, pp. 4146–4164, 2014.

[8] T. Svensson, M. Werner, R. Legouable, T. Frank, and E. Costa, "WINNER II Channel Models," vol. 1, no. 206, pp. 1–206, 2007. [Online]. Available: http://projects.celtic-initiative.org/WINNER+/WINNER2-Deliverables/D4.6.1.pdf

[9] IEEE Computer Society : LAN/MAN Standards Committee, *Part 11: Wireless LAN Medium Access Control (MAC) and Physical Layer (PHY) Specifications, Amendment 6: Wireless Access in Vehicular Environments (WAVE)*, 2010.

[10] Y. Liu, C. Wang, J. Huang, J. Sun, and W. Zhang, "Novel 3-d nonstationary mmwave massive mimo channel models for 5g high-speed train wireless communications," *IEEE Transactions on Vehicular Technology*, vol. 68, no. 3, pp. 2077–2086, March 2019.

[11] S. Wu, C. Wang, e. M. Aggoune, M. M. Alwakeel, and X. You, "A general 3-d non-stationary 5g wireless channel model," *IEEE Transactions on Communications*, vol. 66, no. 7, pp. 3065–3078, July 2018.

[12] M. Arnold, W. H. R. Miltner, H. Witte, R. Bauer, and C. Braun, "Adaptive AR modeling of nonstationary time series by means of Kalman filtering," *IEEE Trans. Biomed. Eng.*, vol. 45, no. 5, pp. 545–552, 1998.

[13] M. Al-Ibadi and A. Dutta, "Predictive analytics for non-stationary v2i channel," in *2017 9th International Conference on Communication Systems and Networks (COMSNETS)*, Jan 2017, pp. 243–250.

[14] X. Wu, S. Subramanian, R. Guha, R. G. White, J. Li, K. W. Lu, A. Bucceri, and T. Zhang, "Vehicular communications using dsrc: Challenges, enhancements, and evolution," *IEEE Journal on Selected Areas in Communications*, vol. 31, no. 9, pp. 399–408, September 2013.

[15] C. F. Mecklenbraüker, A. F. Molisch, J. Karedal, F. Tufvesson, A. Paier, L. Bernadó, T. Zemen, O. Klemp, and N. Czink, "Vehicular channel characterization and its implications for wireless system design and performance," *Proceedings of the IEEE*, vol. 99, no. 7, pp. 1189–1212, 2011.

[16] A. Ghazal, C. Wang, H. Haas, M. Beach, X. Lu, D. Yuan, and X. Ge, "A non-stationary mimo channel model for high-speed train communication systems," in *2012 IEEE 75th Vehicular Technology Conference (VTC Spring)*, May 2012.

[17] J.-q. Chen, Z. Zhang, T. Tang, and Y.-z. Huang, "A non-stationary channel model for 5g massive mimo systems," *Frontiers of Information Technology & Electronic Engineering*, vol. 18, no. 12, pp. 2101–2110, Dec 2017. [Online]. Available: https://doi.org/10.1631/FITEE.1700028

[18] P. Almers, E. Bonek, A. Burr, N. Czink, m. Debbah, V. Degli-Esposti, H. Hofstetter, P. Kyösti, D. Laurenson, G. Matz, A. Molisch, C. Oestges, and H. Özcelik, "Survey of channel and radio propagation models for wireless mimo systems." *EURASIP J. Wireless Comm. and Networking*, vol. 2007, 01 2007.

[19] W. Viriyasitavat, M. Boban, H. Tsai, and A. Vasilakos, "Vehicular communications: Survey and challenges of channel and propagation models," *IEEE Vehicular Technology Magazine*, vol. 10, no. 2, pp. 55–66, June 2015.

[20] C. Wang, J. Bian, J. Sun, W. Zhang, and M. Zhang, "A survey of 5g channel measurements and models," *IEEE Communications Surveys Tutorials*, vol. 20, no. 4, pp. 3142–3168, Fourthquarter 2018.

[21] A. Gehring, M. Steinbauer, I. Gaspard, and M. Grigat, "Empirical Channel Stationarity in Urban Environments," in *Proceedings of the European Personal Mobile Communications Conference*, 2001, talk: 4th European Personal Mobile Communications Conference (EPMCC 2001), Vienna, Austria; 2001-02-20 – 2001-02-22. [Online]. Available: http://publik.tuwien.ac.at/files/pub-et_12758.pdf

[22] M. Herdin, N. Czink, H. Ozcelik, and E. Bonek, "Correlation matrix distance, a meaningful measure for evaluation of non-stationary mimo channels," in *2005 IEEE 61st Vehicular Technology Conference*, vol. 1, May 2005, pp. 136–140 Vol1.

[23] F. Hlawatsch and G. Matz, *Wireless Communications Over Rapidly Time-Varying Channels*, 1st ed. USA: Academic Press, Inc., 2011.

[24] K. Sil, M. Agarwal, D. Guo, M. L. Honig, and W. Santipach, "Performance of turbo decision-feedback detection for downlink OFDM," *IEEE Wireless Communications and Networking Conference, WCNC*, pp. 1488–1492, 2007.

[25] R. Budde and R. Kays, "Delayed decision feedback equalization with adaptive noise filtering for IEEE 802.11p," in *2013 IEEE Vehicular Networking Conference*, Dec 2013, pp. 17–23.

[26] E. P. Simon, H. Hijazi, L. Ros, M. Berbineau, and P. Degauque, "Joint estimation of carrier frequency offset and channel complex gains for ofdm systems in fast time-varying vehicular environments," in *2010 IEEE International Conference on Communications Workshops*, May 2010, pp. 1–5.

[27] J. B. Andersen, J. Jensen, S. H. Jensen, and F. Frederiksen, "Prediction of future fading based on past measurements," in *Gateway to 21st Century Communications Village. VTC 1999-Fall. IEEE VTS 50th Vehicular Technology Conference (Cat. No.99CH36324)*, vol. 1, Sep. 1999, pp. 151–155 vol.1.

[28] T. Zemen, C. F. Mecklenbrauker, F. Kaltenberger, and B. H. Fleury, "Minimum-energy band-limited predictor with dynamic subspace selection for time-variant flat-fading channels," *IEEE Transactions on Signal Processing*, vol. 55, no. 9, pp. 4534–4548, Sep. 2007.

[29] Y. Liao, X. Shen, G. Sun, X. Dai, and S. Wan, "Ekf/ukf-based channel estimation for robust and reliable communications in v2v and iiot," *EURASIP Journal on Wireless Communications and Networking*, vol. 2019, 12 2019.

[30] E. Acar, D. M. Dunlavy, T. G. Kolda, and M. Mørup, "Scalable tensor factorizations for incomplete data," *Chemometrics and Intelligent Laboratory Systems*, vol. 106, no. 1, pp. 41 – 56, 2011, multiway and Multiset Data Analysis. [Online]. Available: http://www.sciencedirect.com/science/article/pii/S0169743910001437

[31] H. Sun, Y. Zhong, and W. Zhang, "Channel selection through a recommender system," in *2010 International Conference on Wireless Communications Signal Processing (WCSP)*, Oct 2010, pp. 1–5.

[32] I. Mashal, O. Alsaryrah, and T. Y. Chung, "Analysis of recommendation algorithms for internet of things," in *2016 IEEE Wireless Communications and Networking Conference Workshops (WCNCW)*, April 2016, pp. 181–186.

[33] L. C. L. Cheng, B. Henty, R. Cooper, D. Stancil, and F. B. F. Bai, "Multi-Path Propagation Measurements for Vehicular Networks at 5.9 GHz," *2008 IEEE Wireless Communications and Networking Conference*, pp. 1239–1244, 2008.

[34] J. Karedal, F. Tufvesson, N. Czink, A. Paier, C. Dumard, T. Zemen, C. F. Mecklenbräuker, and A. F. Molisch, "A geometry-based stochastic MIMO model for vehicle-to-vehicle communications," *IEEE Transactions on Wireless Communications*, vol. 8, no. 7, pp. 3646–3657, 2009.

[35] P. Kyösti, J. Meinilä, L. Hentilä, X. Zhao, T. Jämsä, C. Schneider, M. Narandzic, M. Milojevic, A. Hong, J. Ylitalo, V.-M. Holappa, M. Alatossava, R. J. C. Bultitude, Y. L. C. D. Jong, T. Rautiainen, J. Ebitg, Meinilä, X. Ebitg, Z. Zhao, M. Uoulu, Alatossava, V.-M. Uoulu, Holappa, R. Crc, Bultitude, and C. Y. D. Jong, "Winner ii channel models part i channel models."

[36] D. L. Romero, N. B. Chang, and A. R. Margetts, "Practical non-binary rateless codes for wireless channels," in *2013 Asilomar Conference on Signals, Systems and Computers*, Nov 2013, pp. 2084–2088.

[37] M. A. A. Careem and A. Dutta, "Spatio-temporal recommender for v2x channels," in *2018 IEEE 88th Vehicular Technology Conference (VTC-Fall)*, Aug 2018, pp. 1–7.

[38] M. Verhaegen and P. Van Dooren, "Numerical Aspects of Different Kalman Filter Implementations," *IEEE Trans. Automat. Contr.*, vol. AC-31, no. October, pp. 1–11, 1986.

[39] T. G. Kolda and B. W. Bader, "Tensor decompositions and applications," *SIAM Review*, vol. 51, no. 3, pp. 455–500, 2009. [Online]. Available: https://doi.org/10.1137/07070111X

[40] E. J. Candès and T. Tao, "The power of convex relaxation: Near-optimal matrix completion," *CoRR*, vol. abs/0903.1476, 2009. [Online]. Available: http://arxiv.org/abs/0903.1476

[41] C. Montella, "The kalman filter and related algorithms: A literature review," 05 2011.

[42] A. Phan, P. Tichavský, and A. Cichocki, "Candecomp/parafac decomposition of high-order tensors through tensor reshaping," *IEEE Transactions on Signal Processing*, vol. 61, no. 19, pp. 4847–4860, Oct 2013.

[43] M. C. S. T. Team, "Winner ii channel model for communications system toolbox," Available online, October 2016. [Online]. Available: https://www.mathworks.com/matlabcentral/fileexchange/59690-winner-ii-channel-model-for-communications-system-toolbox

[44] S. Jaeckel, L. Raschkowski, K. Börner, and L. Thiele, "Quadriga: A 3-d multi-cell channel model with time evolution for enabling virtual field trials," *IEEE Transactions on Antennas and Propagation*, vol. 62, no. 6, pp. 3242–3256, June 2014.

[45] "How does connected vehicle technology work." [Online]. Available: https://www.its.dot.gov/cv_basics/cv_basics_how.htm

[46] A. McQuinn and D. S. Castro, "A policymaker's guide to connected cars." Innovation Technology and Information Foundation, 2018.

[47] T. L. Willke, P. Tientrakool, and N. F. Maxemchuk, "A survey of inter-vehicle communication protocols and their applications," *IEEE Communications Surveys Tutorials*, vol. 11, no. 2, pp. 3–20, 2009.

[48] LAN/MAN Standards Committee, S. Committee, and I. Computer, *Part 11 : Wireless LAN Medium Access Control (MAC) and Physical Layer (PHY) S pecifications*, 2012, vol. 2012, no. March.

[49] S. Coleri, M. Ergen, A. Puri, and A. Bahai, "Channel estimation techniques based on pilot arrangement in OFDM systems," in *Broadcasting, IEEE Transactions on*, vol. 48, pp. 223–229.

[50] S. Sur, R. Bera, and B. Maji, "Feedback equalizer for vehicular channel," *International Journal on Smart Sensing and Intelligent Systems*, vol. 10, pp. 50–68, 03 2017.

[51] A. Goldsmith, *Wireless Communications*. New York, NY, USA: Cambridge University Press, 2005.